PHYSICAL REVIEW D **96,** 035036 (2017)

Harmonizing the MSSM with the Galactic Center excess

Anja Butter,[1] Simona Murgia,[2] Tilman Plehn,[1] and Tim M. P. Tait[2]
[1]*Institut für Theoretische Physik, Universität Heidelberg, 69120 Heidelberg, Germany*
[2]*Department of Physics and Astronomy, University of California, Irvine, California 92697, USA*
(Received 7 March 2017; published 31 August 2017)

The minimal supersymmetric setup offers a comprehensive framework to interpret the Fermi-LAT Galactic Center excess. Taking into account experimental, theoretical, and astrophysical uncertainties we can identify valid parameter regions linked to different annihilation channels. They extend to dark matter masses above 250 GeV. There exists a very mild tension between the observed relic density and the annihilation rate in the center of our Galaxy for specific channels. The strongest additional constraints come from the new generation of direct detection experiments, ruling out much of the light and intermediate dark matter mass regime and giving preference to heavier dark matter annihilating into a pair of top quarks.

DOI: 10.1103/PhysRevD.96.035036

I. INTRODUCTION

While the existence of an unknown dark matter as the primary matter component of today's Universe is solidly established, its particle nature remains elusive. A broad experimental program seeks to shed light on this question by searching for dark matter indirectly through the products of its annihilation, directly scattering with terrestrial targets, or being produced at colliders. Among indirect searches, gamma rays with GeV-range energies are a particularly effective messenger because they propagate unhindered on galactic scales, and thus can be effectively traced back along the direction of their origin. In recent years, the Fermi Large Area Telescope (Fermi-LAT) has mapped out the gamma-ray sky with unprecedented resolution, leading to the current best limits on the annihilation cross section for dark matter particles with masses around 100 GeV.

Remarkably, the Fermi-LAT data contains an indication of what appears to be an excess of gamma rays from the direction of the Galactic Center (GC) above the predictions from astrophysical models, with spatial morphology and spectrum consistent with expectations for the annihilation of a thermal relic [1–3]. The Fermi-LAT Collaboration has released its own analysis [4] of the gamma rays from the direction of the GC based on specialized interstellar emission models (IEMs). These models allow for a determination of the gamma-ray fore/background originating from cosmic rays interacting with the interstellar gas and radiation field, and for a separation from the contribution from within roughly 1 kpc of the GC along the line of sight toward it. The GC excess persists in this analysis, and its spectral properties display a strong dependence on the assumed IEM, making it challenging to conclusively identify its origin. It thus remains unclear whether this signal arises from dark matter annihilation rather than from other, more mundane sources, such as a population of unresolved millisecond pulsars, cosmic-ray proton or electron outbursts, additional cosmic-ray sources, and/or emission from a stellar overdensity in the Galactic bulge [5]. An interesting development is the use of statistical tools which indicate that the excess displays more clustering than would be expected from Poisson noise from smooth components [6]. However, it remains difficult with the current models to disentangle whether this feature represents a property of the excess itself, or unmodeled variation in the background components [7].

While it is premature to claim that the GC excess represents a confirmed signal of dark matter annihilation, in this paper we interpret its properties under the assumption that it does in the framework of the minimal supersymmetric extension of the Standard Model (MSSM). The MSSM is a prototypical model of weakly interacting massive particles. In the region of parameter space for which the lightest supersymmetric particle (LSP) is a neutralino, a rich vision for dark matter emerges, largely dictated by its component fractions of electroweak singlet, doublet, and triplet representations [8]. Despite this flexibility, it is somewhat challenging to fit the original characterizations of the GC excess in the MSSM (though viable parameter space does exist [9,10]) due to the generic requirement of efficient mediators [11]. Such mediators are naturally present in extended models such as the NMSSM [12–14].

In this article, we perform the first analysis of the MSSM parameter space capable of describing the GC excess as extracted by the Fermi-LAT Collaboration in Ref. [4], including the range of spectra corresponding to the full suite of models for the interstellar emission developed therein. We examine how this wide range of spectra opens up regions of the MSSM parameter space describing the excess [15] by performing global fits to these spectra in the SFitter framework [16], consistently with the thermal relic density, the light Higgs boson mass, and the standard set of low energy indirect constraints. The power of such a global analysis rests in its ability to interpret the wide range of relevant experimental observations [17–20].

II. THE GALACTIC CENTER EXCESS

The Fermi-LAT Collaboration determination of the GC excess is based on the first 62 months of data in a $15° \times 15°$ region in the direction of the GC in the energy range $E_\gamma = 1 \ldots 100$ GeV. In order to minimize the bias from the data toward the GC, the methodology developed in Ref. [4] employs regions outside of the $15° \times 15°$ region for the determination of the fore/background emission. Furthermore, the point sources are determined self-consistently together with each IEM. This is a crucial improvement over previous analyses, as the determination of the point sources in this region is strongly dependent on the IEM. We refer the reader to Ref. [4] for a more detailed description of these models and their associated point sources.

We adopt the Fermi-LAT GC excess spectrum for a spectral model assumed to be a power-law function in each of 10 energy bands, equally spaced in logarithmic energy over $E_\gamma = 1 \ldots 100$ GeV, shown in Fig. 1. The obtained spectral envelope spans the full set of IEMs and therefore encompasses the interstellar emission modeling uncertainty from Ref. [4], uncorrelated bin-by-bin in the energy spectrum. Unlike a correlated global modification, this allows for a more sizable change in the shape of the photon spectrum. The exclusive log-likelihood is flat within the envelope, in harmony with the assumption for theoretical uncertainties in SFitter [16]. Combined with a profile likelihood this is equivalent to using the RFit scheme [21]. In addition to the modeling uncertainty on the interstellar emission, which is the dominant source of uncertainty, we include the statistical error on the signal rate after background subtraction. The statistical uncertainty thus reflects the combined statistical uncertainty of both of signal and background [16], and it is uncorrelated between bins. Furthermore, we include a 10% uncertainty from the fragmentation function for photons [19], treated as uncorrelated between energy bins and Gaussian distributed. Finally, we include the systematic error on the Fermi-LAT effective area [22], treated as fully correlated between bins and also Gaussian distributed.

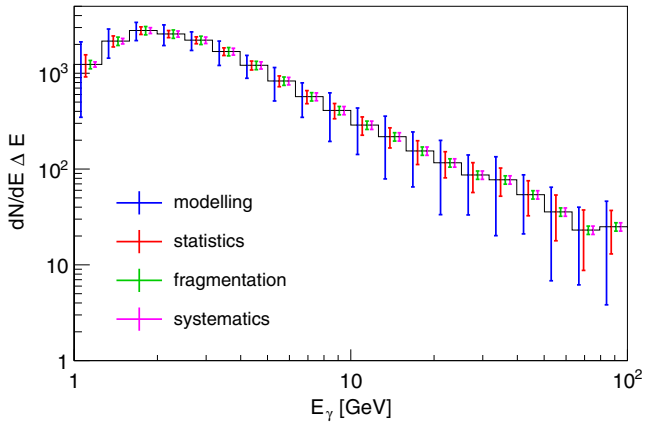

FIG. 1. GC excess spectrum from [4], including uncertainties from the interstellar emission model and fragmentation, as well as instrumental systematics and statistical uncertainties, as described in the text.

The primary observables for the GC excess are the annihilation cross section, which characterizes the overall brightness of the excess, and its spectral shape binned in energy. The annihilation cross section itself is fully degenerate with the J-factor, which quantifies the integral of the square of the dark matter density along the line of sight encompassed within the $15° \times 15°$ region employed to extract the signal in Ref. [4]. The best estimates for the uncertainty in the J-factor are that it can vary by roughly a factor of 2 in the region of interest [23].

III. MSSM ANNIHILATION CHANNELS

Our MSSM parameter analysis can be most easily organized in terms of the dominant dark matter annihilation channels. For a typical weakly interacting dark matter candidate comprising all of the dark matter and following a standard cosmological history, the same annihilation cross section which explains the GC excess also determines the thermal relic abundance. However, in a theory containing multiple components of dark matter and/or a nonstandard cosmology, the relic abundance and the annihilation cross section are less correlated. For this reason, in this section we remain somewhat agnostic as to whether the dark matter abundance arises from the usual freeze-out calculation, whereas in Sec. IV we fit both the GC excess and the relic abundance assuming a standard cosmological history.

We focus on the most important MSSM parameters determining the dark matter properties: the wino mass M_2, the Higgsino mass parameter μ, and the bino mass M_1. As we will see below, the masses of the heavy Higgs states $m_{A,H}$ can play an important role for dark matter annihilation. The light Higgs mass m_h is adjusted with the help of $\tan\beta$, A_t. The third-generation squark masses, with the remaining sleptons, squarks, and gluinos are assumed to decouple, as suggested by the Higgs mass and the direct limits from the null results of LHC searches. For all scenarios we require the light Higgs mass to match roughly the measured value $m_h = 125$ GeV and charginos to be heavier than the LEP limit of 103 GeV.

For the purpose of this analysis the Higgs mass is mainly relevant as a possible mediator in the dark matter annihilation. As its exact value is not important for our analysis we choose a flat uncertainty of 3 GeV to avoid any potential unrealistic numerical fine-tuning. Since we used the freedom to adjust the stop mass parameters for each of the fits such that the mass of the Higgs boson would be around 125 GeV, the variation of the fitted parameters usually leads to deviations smaller than 1 GeV within the displayed parameter space. A reduction of the assigned uncertainty therefore could only result in a very minor change of shape.

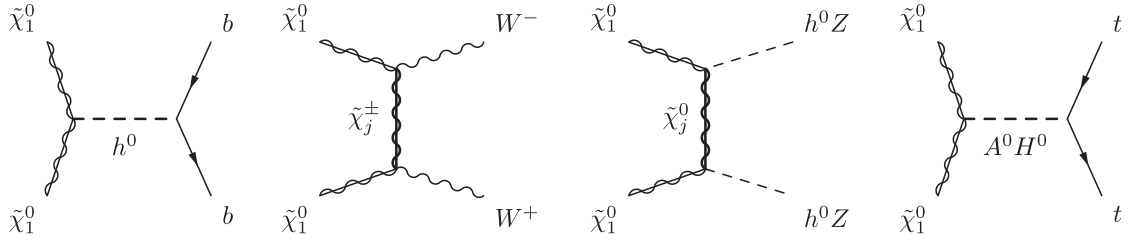

FIG. 2. Feynman diagrams illustrating dark matter annihilation $\tilde{\chi}_1^0\tilde{\chi}_1^0 \to b\bar{b}, WW, ZZ, hh, t\bar{t}$ in the MSSM.

As for all SFitter analyses [16] we calculate the MSSM spectrum with SuSpect3 [24], while the Higgs branching ratios are computed using Susy-Hit and HDecay [25]. The relic density and the indirect annihilation rate are calculated with MicrOMEGAs [26].

Representative Feynman diagrams for the most important annihilation processes are shown in Fig. 2. Generically, it is difficult to realize large enough cross sections to explain the GC excess [17,27,28] for an LSP with a suitable mass. For example, t-channel annihilation channels are generally not very efficient and decouple rapidly with the mediator mass [29]. Large enough annihilation cross sections typically occur for

(i) t-channel chargino exchange driven by the coupling to W-bosons in the final state,

$$g_{W\tilde{\chi}_1^0\tilde{\chi}_1^+} = \frac{g\sin\theta_w}{\cos\theta_w}\left(\frac{1}{\sqrt{2}}N_{14}V_{12}^* - N_{12}V_{11}^*\right), \quad (1)$$

which is most efficient for charginos just above the LEP limit $m_{\tilde{\chi}_1^+} = 103$ GeV. A substantial coupling to W-bosons requires that the LSP contains a sizable fraction of either a wino Higgsino fraction.

(ii) t-channel neutralino exchange, leading to $\tilde{\chi}_1^0\tilde{\chi}_1^0 \to ZZ$ or $\tilde{\chi}_1^0\tilde{\chi}_1^0 \to hh$ [3]. For the former, the relevant coupling is an axial-vector coupling with strength

$$g_{Z\tilde{\chi}_1^0\tilde{\chi}_i^0} = \frac{g}{2\cos\theta_w}(N_{13}N_{i3} - N_{14}N_{i4}), \quad (2)$$

driven by the Higgsino content. For the latter process, the relevant couplings are products of Higgsino and gaugino fractions, requiring that the LSP be a highly mixed state,

$$g_{h\tilde{\chi}_1^0\tilde{\chi}_1^0} = (g'N_{11} - gN_{12})(\sin\alpha N_{13} + \cos\alpha N_{14}). \quad (3)$$

The mixing angle α describes the rotation of the scalar Higgses into mass eigenstates.

(iii) t-channel sfermion exchange, e.g., tau sleptons. In this case, significant coupling requires a large wino fraction, which typically leads to excessively large annihilation into W-bosons for LSP masses below around 1 TeV.

More efficient are s-channel annihilation processes, particularly when the masses of the dark matter and the mediating particle are arranged such that the annihilation benefits from the on-shell resonance. Candidates for s-channel mediators in the MSSM are

(i) Vector Z-funnel annihilation through the Higgsino component, as illustrated in Eq. (2). The coupling vanishes in the limit $\tan\beta \to 1$, due to approximately equal Higgsino fractions. Large $\tan\beta$ also reduces the predicted spin-independent direct detection cross section and therefore allows for a larger allowed parameter space. Because the axial-vector component does not have a velocity suppression, the annihilation rate $\langle\sigma v\rangle$ usually prefers LSP masses slightly above or below 45 GeV; directly on the Z pole the annihilation is too efficient.

(ii) Scalar h-funnel annihilation, where the LSP mass should be around $m_{\tilde{\chi}_1^0} = 63$ GeV, slightly away from the resonance. The coupling in Eq. (3) relies on Higgsino-gaugino mixing. Almost the entire neutralino annihilation rate through the light Higgs funnel goes to $b\bar{b}$, with small contributions or $\tau^+\tau^-$ and WW.

(iii) Heavy (pseudo-)scalar Higgs funnel annihilation, where the pseudoscalar A^0 leads to an efficient s-wave annihilation. The coupling is again driven by Higgsino-gaugino mixing. Heavy scalar decays to down-type fermions are enhanced by $\tan\beta$, which implies that for $\tan\beta \gtrsim 30$ the resonance pole structure of the A funnel gets significantly washed out and a $b\bar{b}$ final state appears from this topology.

Finally, coannihilation channels are an efficient means to realize the relic density when there is an additional supersymmetric particle within about 10% of the LSP mass [30–32]. For the light dark matter particles, usually associated with the Fermi-LAT GC excess, additional light charginos or sfermions are strongly disfavored for example by LEP constraints [33]. For heavier dark matter, coannihilation can significantly contribute for example for processes with a light chargino in the t channel.

The above annihilation mechanisms are often closely linked to LHC search channels. For instance, t-channel chargino annihilation or neutralino/chargino coannihilation point to more than one light electroweakino, where at least one of the additional light states is a chargino. In this

situation one can search for $\tilde{\chi}_j^0\tilde{\chi}_1^\pm$ or $\tilde{\chi}_1^+\tilde{\chi}_1^-$ production. One of the classic signatures are tri-leptons, which become challenging when the mass differences between the chargino and the neutralino become small [34]. Similarly, t-channel sfermion exchange or sfermion coannihilation point towards another light particle, which can be pair produced through its QED or QCD interactions. As long as the mass difference is not extremely small, such light sfermions are accessible at the LHC, particularly when colored. The situation becomes more challenging when the mediator is a Standard Model particle. To establish this mediator role one would need to establish Z or Higgs coupling to the dark matter sector, for example through invisible Z [35] and/or Higgs decays [36].

$$\chi\chi \to b\bar{b}$$

To define an MSSM scenario with a light neutralino responsible for the GC excess we examine the regions of MSSM parameter space where the annihilation $\tilde{\chi}_1^0\tilde{\chi}_1^0 \to b\bar{b}$ dominates the dark matter annihilation in Fig. 3. For light neutralinos, annihilation tends to be dominated by the s-channel light Higgs funnel, rather than the broad A-induced band. The lightest neutralino is mostly bino, with some Higgsino content to couple to the Z and the light Higgs mediators, and negligible wino content ($M_2 = 700$ GeV). We also fix $\tan\beta = 45$, though the results are rather insensitive to this choice. The varying neutralino mass on the x axis is generated by adjusting M_1 for each of the fixed values of μ.

On the left y axis in the left panel of Fig. 3 we show the inverse relic density, proportional to the annihilation rate in the early universe. The corresponding solid curves exhibit two distinct peaks, one for Z-funnel annihilation and one for h-funnel annihilation. For both peaks the width is given by the velocity spectrum rather than the intrinsic width of the mediators. The enhancement of the two peaks over the continuum end up being comparable, with the Z funnel coupled to the axial-vector current which is velocity suppressed with $v \lesssim 1/10$, whereas the Higgs funnel is suppressed by the small bottom Yukawa coupling. The measured relic density can be reproduced on the shoulders of the resonance peaks, with a slight preference for larger μ values and hence smaller couplings.

On the right y axis of Fig. 3 (corresponding to the dashed curves) we show the annihilation rate in the GC, with the rough target rate indicated by the horizontal line. Because of the much smaller velocities, the widths of the resonance peaks are now determined by the physical widths of the Z and the Higgs. The Higgs resonance leads to much larger peak rates, because of the stronger velocity suppression of the axial-vector coupling to the Z mediator. We observe that continuum as well as the reduced Z-pole annihilation are not capable of explaining the GC excess, but the light Higgs pole scans through the required cross section.

In the right panel of Fig. 3 we show a zoomed-in version of the Higgs peak. The interesting parameter regions for a combined fit of the relic density with the GC excess will be given by the solid relic density curves crossing the solid horizontal line and the dashed GC lines crossing the dashed horizontal line. As expected from the left panel, there are finely tuned regions around the Higgs pole with today's velocity spectrum, which allow for an explanation of the GC excess via a thermal relic through the process $\tilde{\chi}_1^0\tilde{\chi}_1^0 \to b\bar{b}$. Decays of the light Higgs mediator to lighter fermions, like tau leptons, are subleading because of the smaller Yukawa coupling and the smaller color factor. Annihilation through a t-channel stau generally results in an annihilation rate which is too small.

$$\chi\chi \to WW$$

At slightly larger LSP masses, the dominant neutralino annihilation channel is $\tilde{\chi}_1^0\tilde{\chi}_1^0 \to WW$, mediated by a light

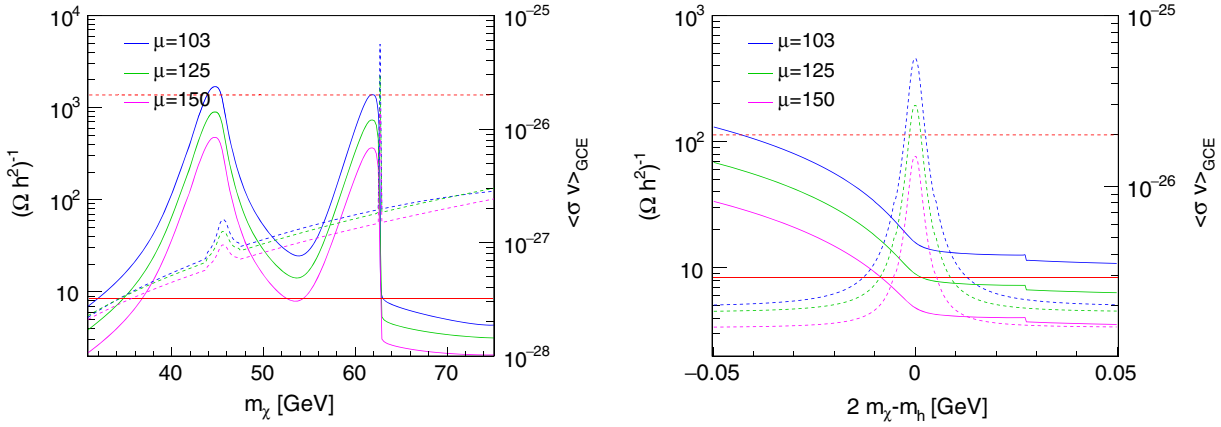

FIG. 3. Inverse relic density (dashed, left axis) and annihilation rate in the GC (solid, right axis) for an MSSM parameter point where the annihilation is dominated by $\tilde{\chi}_1^0\tilde{\chi}_1^0 \to b\bar{b}$. The right panel is zoomed into the Higgs pole region. Additional model parameters are $\tan\beta = 45$, and third-generation squark masses range around 1 TeV.

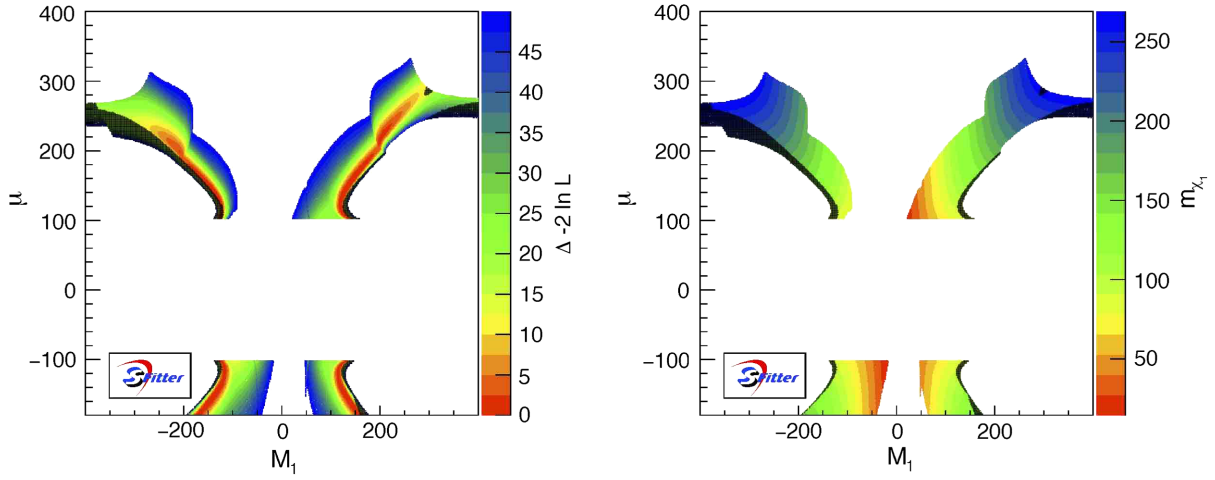

FIG. 4. Log-likelihood map (left) and corresponding LSP mass (right) based on the Fermi-LAT photon spectrum for $M_2 = 700$ GeV and $\tan\beta = 45$, where $\tilde{\chi}_1^0\tilde{\chi}_1^0 \to WW$ is a dominant annihilation channel. The heavy Higgses are decoupled to 1 TeV. The shaded dots are excluded by the Fermi-LAT limits from dwarf spheroidal galaxies.

chargino in the t channel (and chargino-neutralino coannihilation for the relic density). Equation (1) indicates that either wino or Higgsino LSP content enhances this annihilation rate. In Fig. 4 we show the regions of the M_1-μ plane explaining the GC excess. Here, SFitter determines multidimensional likelihood maps for the model parameter space. A set of Markov chains selects points in the model space following a Breit-Wigner proposal function. For each point we compute all considered observables and determine a generalized χ^2 value [16,20]. For this first analysis the likelihood map is 2 dimensional, covering M_1 and μ over the range defined in the figures. We fix $M_2 = 700$ GeV, implying that the LSP is a mixture of Higgsino, coupling to electroweak bosons, and bino. The preferred parameter range compensates an increase in $|\mu|$ by an increase in M_1. This way the sizeable Higgsino content survives, while the neutralino mass increases, as can be seen in the right panel of Fig. 4. In the lower bands the allowed LSP masses extend to $m_{\tilde{\chi}_1^0} \approx 150$ GeV, without much decrease in the log-likelihood. The change in shape around $M_1 = |\mu| = 200$ GeV is caused by the onset of the annihilation to top pairs. The MSSM parameter regions which allow for efficient annihilation in gauge bosons are strongly correlated in M_1 and μ, but not as tuned as the light Higgs funnel region with its underlying pole condition. Technically, this means that they are easy to identify in a global fit. In Fig. 4 we also indicate the Fermi-LAT limits from dwarf spheroidal galaxies [37] as black dots. While these constraints are visible in the M_1 vs μ plane, they do not significantly interfere with the best-fit regions from the GC excess.

$\chi\chi \to t\bar{t}$

Large annihilation cross sections for $\tilde{\chi}_1^0\tilde{\chi}_1^0 \to t\bar{t}$ can be accomplished by decreasing the heavy pseudoscalar mass to $m_A = 500$ GeV and increasing the effective top Yukawa coupling by choosing $\tan\beta = 3$. We show the allowed parameter range for heavy winos, $M_2 = 700$ GeV, in Fig. 5. From Fig. 4 we observe that for $m_{\tilde{\chi}_1^0} > 175$ GeV the annihilation into top pairs follows the WW annihilation region in the M_1-μ plane. We note that the WW now behaves exactly the same way, in spite of the lower choice of $\tan\beta$.

The primary difference is smaller M_1 values around $|\mu| = 200$ GeV. This increased bino fraction compensates the fact that the underlying top Yukawa coupling is larger than the weak gauge coupling. According to Fig. 5 the allowed mass range now extends to $m_{\tilde{\chi}_1^0} \gtrsim 200$ GeV. The main new feature for the reduced value of $m_A = 500$ GeV is the peak towards large μ values for $M_1 \approx 300$ GeV. The corresponding LSP mass is around 250 GeV, close to the A pole. On the pole, annihilation is too efficient and the preferred coupling is reduced by a smaller Higgsino fraction in the LSP. Beyond the pole, the allowed region extends to LSP masses above 250 GeV, but with a reduced log-likelihood. If we choose larger values of $\tan\beta$ the same structure remains, but the narrow pole gets washed out into a wider band of dark matter masses. The fact that this large-$|M_1|$ regime does not appear in the upper left corner of Fig. 5 is explained by the default SuSpect setup, where this region of parameter space can lead to $m_{\tilde{\chi}_1^+} < m_{\tilde{\chi}_1^0}$. However, an appropriate renormalization scheme like for example an on-shell scheme for the lightest three neutralinos/charginos ensures that the tree-level hierarchy $m_{\tilde{\chi}_1^+} > m_{\tilde{\chi}_1^0}$ remains intact at loop level [38].

$\chi\chi \to hh$

In principle, for $m_{\tilde{\chi}_1^0} > m_h$ the LSP can also annihilate to a pair of SM-like Higgs bosons, $\tilde{\chi}_1^0\tilde{\chi}_1^0 \to hh$. While the

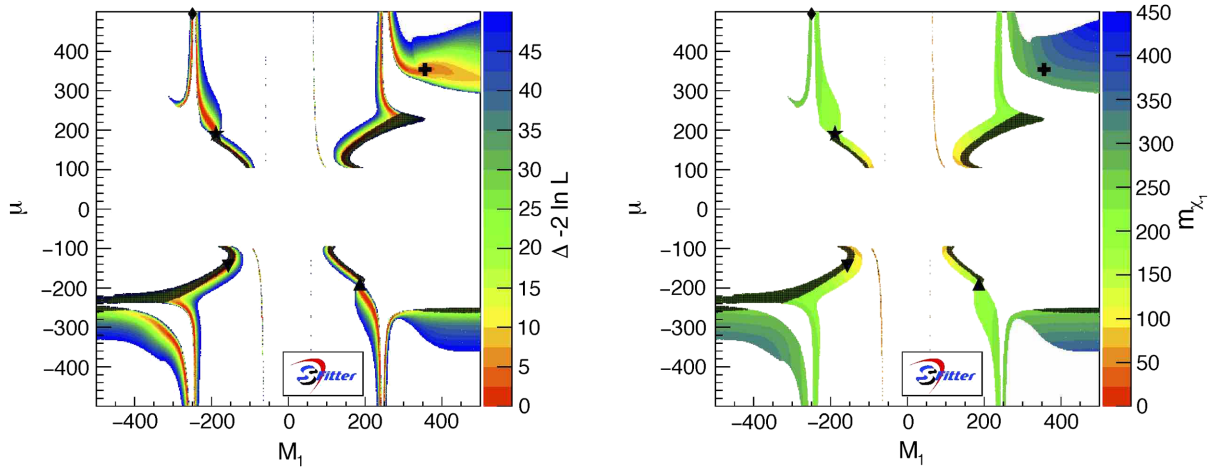

FIG. 5. Log-likelihood map (left) and corresponding LSP mass (right) based on the Fermi-LAT photon spectrum for $M_2 = 700$ GeV, $\tan\beta = 3$, and $m_A = 500$ GeV, where we also observe the annihilation $\tilde{\chi}_1^0\tilde{\chi}_1^0 \to t\bar{t}$. The shaded dots are excluded by the Fermi-LAT limits from dwarf spheroidal galaxies. The five symbols indicate local best-fitting parameter points.

t-channel neutralino diagram will typically be overwhelmed by the annihilation to weak bosons with the same t-channel mediator, an s-channel mediator with $m_{\text{med}} \approx 2m_h$ can dominate for small $\tan\beta$. In Fig. 6 we show the corresponding effect for dark matter annihilation in the early universe (left axis) and in the GC (right axis), similar to the $b\bar{b}$ case in Fig. 3. The LSP mass is varied through M_1, while $\mu = -300$ GeV and $M_2 = 700$ GeV. The heavy Higgses are light, namely $m_A = 300$ GeV and $m_H \approx 320$ GeV. The heavy Higgs' branching ratio to a pair of light Higgses is $\text{BR}(H \to hh) = 30\%$ [39]. For comparably large velocities we see how both s-channel mediators, H and A, contribute through their respective on-shell configuration. In contrast, for the smaller velocities associated with the Fermi-LAT GC excess the CP-odd mediator A completely dominates,

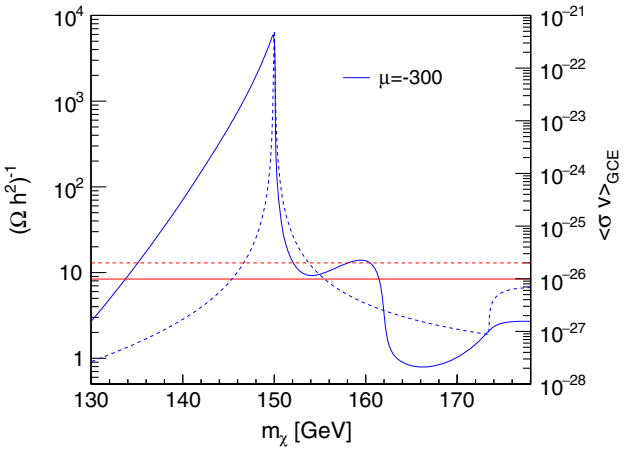

FIG. 6. Inverse relic density (dashed, left axis) and annihilation rate in the GC (solid, right axis) for an MSSM parameter point where the annihilation receives a contribution from $\tilde{\chi}_1^0\tilde{\chi}_1^0 \to hh$.

while the CP-even H does not contribute visibly. Because only the latter couples to two light Higgs bosons, the annihilation to Higgs pairs leading to the GC excess is difficult to realize in the MSSM. This outcome is different from the case of a single-scalar Higgs portal model [40]. The increase we observe in Fig. 6 for $m_{\tilde{\chi}_1^0} > 170$ again shows the onset of the annihilation into two tops.

Based on these example scenarios it is now clear that the GC excess can be realized by the dominant annihilation channels

$$\tilde{\chi}_1^0\tilde{\chi}_1^0 \to b\bar{b}, WW, t\bar{t} \tag{4}$$

in more or less finely tuned parameter ranges of the MSSM. At this level, the assumed value of $\tan\beta$ plays a role in how hard it is to arrive at the correct light Higgs mass and how often the heavy Higgses decay to up-type and down-type fermions. Annihilation to light fermions like $b\bar{b}$ is realized through a finely tuned, resonant s-channel mediator. In addition, the LSP can be a neutralino with $m_{\tilde{\chi}_1^0} = 100\ldots350$ GeV with dominant annihilation to WW and/or $t\bar{t}$ pairs. In Fig. 7 we show a set of sample energy spectra for different scenarios, defined as five local best-fitting points in Fig. 5. We overlay the Fermi-LAT spectrum shown in Fig. 1. The three scenarios with leading decays to $b\bar{b}$, WW, and $t\bar{t}$ shown in the left panel agree with the Fermi-LAT results similarly well. The lowest-energy and highest-energy bins cause the largest problem in particular for a light LSP with Higgs funnel annihilation into $b\bar{b}$ pairs. In the right panel of Fig. 7 we show three different parameter points, all with a leading annihilation to $t\bar{t}$ pairs, and with LSP masses $m_{\tilde{\chi}_1^0} = 180$, 255, and 320 GeV. The overall agreement with the Fermi-LAT spectrum gets slightly worse towards larger masses, leading to a Gaussian-equivalent $\Delta\chi^2 = 4$ between the three curves.

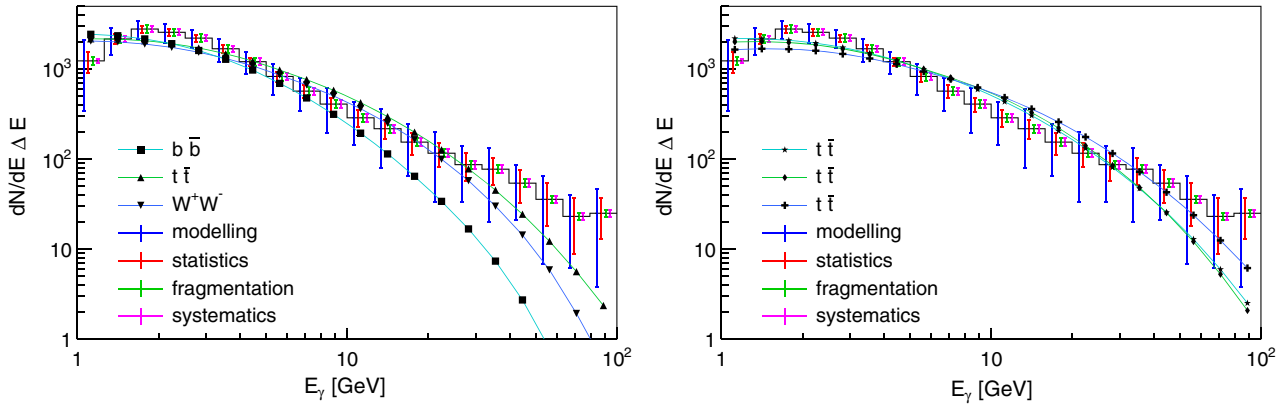

FIG. 7. Spectra for local best-fitting MSSM parameter points, assuming dark matter annihilation dominantly to $b\bar{b}$, WW, $t\bar{t}$ (left) and for three different $t\bar{t}$ annihilation channels (right). The markers correspond to Fig. 5, as indicated.

IV. MSSM ANALYSIS

After understanding how different annihilation channels can be realized in the MSSM we now perform a global analysis to determine the range of MSSM parameter space which can best describe the GC excess. This will be in the context of an LSP which makes up the entirety of the dark matter and whose abundance is set by freeze-out in a standard cosmology. We impose the constraints shown in Table I by generating the MSSM spectrum and the B observables, and $(g-2)_\mu$ with SuSpect3 [24]. The relic density, indirect detection rates, and direct detection rates are extracted from MicrOMEGAs [26]. For $m_{\tilde{\chi}_1^0} < 45$ GeV the additional contribution to the invisible Z width [35] from decays into pairs of LSPs plays a role [14], but in this analysis we do not have to take it into account. The top mass is fixed as an input, because the effect from the small range of values consistent with collider measurements can be absorbed into small shifts in the stop parameters. Limits from direct detection experiments Xenon [41], LUX [42], and PandaX [43], are only applied in the second part of this section.

In the upper two panels of Fig. 8 we show the allowed parameter range in the bino and Higgsino mass parameters, fixing the wino mass to be essentially decoupled $M_2 = 700$ GeV and also decoupling the heavy Higgses. The upper left panel mainly shows the WW and $b\bar{b}$ annihilation regions; in contrast to Fig. 4 we also show the parameter points which give the correct relic density $\Omega_\chi h^2$, quoted in Table I. From Fig. 3 and Fig. 4 we observe that the LSP masses in the $b\bar{b}$ scenario are very close to $m_{\tilde{\chi}_1^0} = m_h/2$, while for the WW scenario they extend to around $m_{\tilde{\chi}_1^0} \approx 150$ GeV. As expected from the similar underlying cross sections, the relic density and the GC excess point to similar parameter regions, with slightly larger μ for the relic density and hence smaller annihilation cross sections $\langle\sigma v\rangle$.

In the upper right panel of Fig. 8 we show the result of a properly combined analysis of the GC excess and the measured relic density. Because of the significantly smaller error bars, the relic density measurement dominates the combined structures in the M_1 vs μ parameter space. We observe three different annihilation mechanisms: the vertical Higgs-pole $b\bar{b}$ peaks for small M_1, the WW region extending diagonally to $M_1 \approx 200$ GeV, and a continuum $t\bar{t}$ region for even larger values of M_1.

In the two lower panels of Fig. 8 we show the same parameters, but including a pseudoscalar with $m_A = 500$ GeV. The left panel illustrates the s-channel annihilation regime and in particular above the A pole the relic density and the GC excess are difficult to reconcile. In the right panel we show how the combined fit follows the relic density contours with its much smaller uncertainties. This also implies that the asymmetry in the left panel with the

TABLE I. Data used for the fit including their systematic, statistical, and theoretical uncertainties, as appropriate.

Measurement	Value	
m_h	$(125.09 \pm 0.21_{\text{stat}} \pm 0.11_{\text{syst}} \pm 3.0_{\text{theo}})$ GeV	[44,45]
$\Omega_\chi h^2$	$0.1188 \pm 0.0010_{\text{stat}} \pm 0.0120_{\text{theo}}$	[46]
a_μ	$(287 \pm 63_{\text{exp}} \pm 49_{\text{SM}} \pm 20_{\text{theo}}) \times 10^{-11}$	[47]
$\text{BR}(B \to X_s\gamma)$	$(3.43 \pm 0.21_{\text{stat}} \pm 0.07_{\text{syst}}) \times 10^{-4}$	[48]
$\text{BR}(B_s^0 \to \mu^+\mu^-)$	$(3.2 \pm 1.4_{\text{stat}} \pm 0.5_{\text{syst}} \pm 0.2_{\text{theo}}) \times 10^{-9}$	[49]
$m_{\chi_1^+}$	>103 GeV	[33]

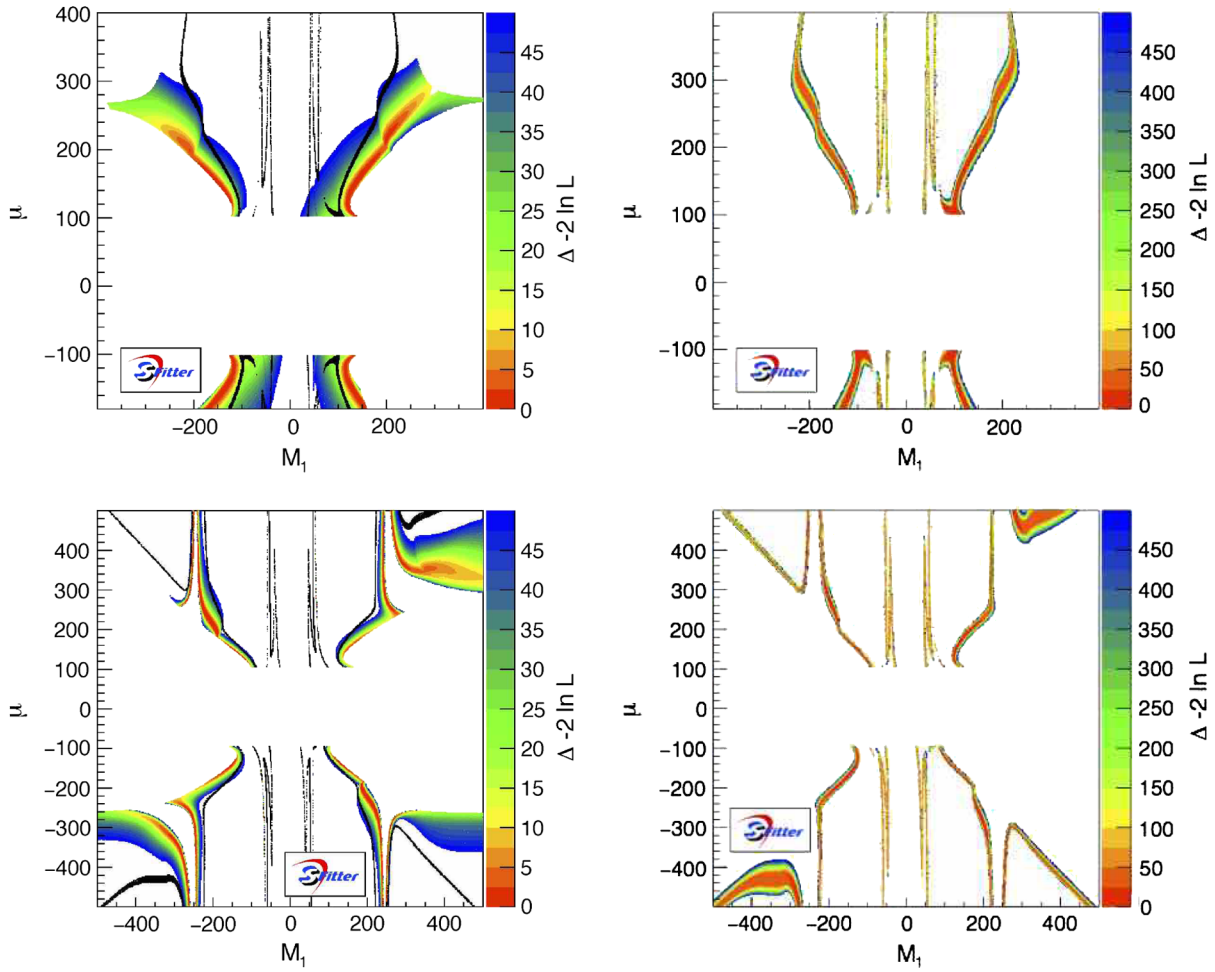

FIG. 8. Log-likelihood map including the Fermi-LAT photon spectrum and the Fermi-LAT limits from dwarf spheroidal galaxies only (left) and in combination with the observed relic density, and other constraints (right) discussed in the text. We fix $M_2 = 700$ GeV, $m_A = 1$ TeV, $\tan\beta = 45$ (upper) or $m_A = 500$ GeV, $\tan\beta = 3$ (lower), and vary M_1 and μ. The black dots in the left panels are roughly compatible with the observed relic density.

missing region at large negative M_1 and large positive μ reappears in the combined fit. Here the problem with $m_{\tilde{\chi}_1^0} > m_{\tilde{\chi}_1^+}$ does not occur.

A. Direct detection

An important, recently improved constraint comes from the direct detection experiments probing coherent spin-independent scattering of dark matter with a heavy nucleus. In the left panel of Fig. 9 we show the combination of the Fermi-LAT GC excess and different direct detection constraints, not including the observed relic density and hence allowing for a nonstandard cosmology. Three shades indicate constraints from Xenon100 [41] (light), PandaX [43] (medium), and LUX [42] (dark). These constraints are included at face value rather than in terms of a combined log-likelihood. Instead of a notoriously difficult error bar, we show three different rounds of exclusion limits to illustrate the possible effect of weaker direct detection constraints. The remaining parameter points are colored according to their combined Fermi-LAT GC excess and indirect constraints log-likelihood. All of the surviving parameter points rely on the annihilation process $\tilde{\chi}_1^0\tilde{\chi}_1^0 \to t\bar{t}$. The reason is that the heavy (pseudo-)scalar mediator does not couple strongly to the nonrelativistic proton content, leaving the corresponding explanation of the GC excess untouched.

For the right panel of Fig. 9 we combine the Fermi-LAT GC excess, direct detection constraints, the observed relic density, and the other constraints shown in Table I. As shown before, the preferred regions in the $M_1 - \mu$ plane are now slightly shifted and defined by the correct prediction of the relic density. With this modification, the A funnel with an annihilation to $t\bar{t}$ as well as a small range of points with the annihilation signature $\tilde{\chi}_1^0\tilde{\chi}_1^0 \to WW$ remain after direct detection constraints. Throughout our analysis we only show log-likelihood differences, the best-fit regions typically lead to a Gaussian equivalent of $\chi^2/\text{d.o.f} \approx 1$.

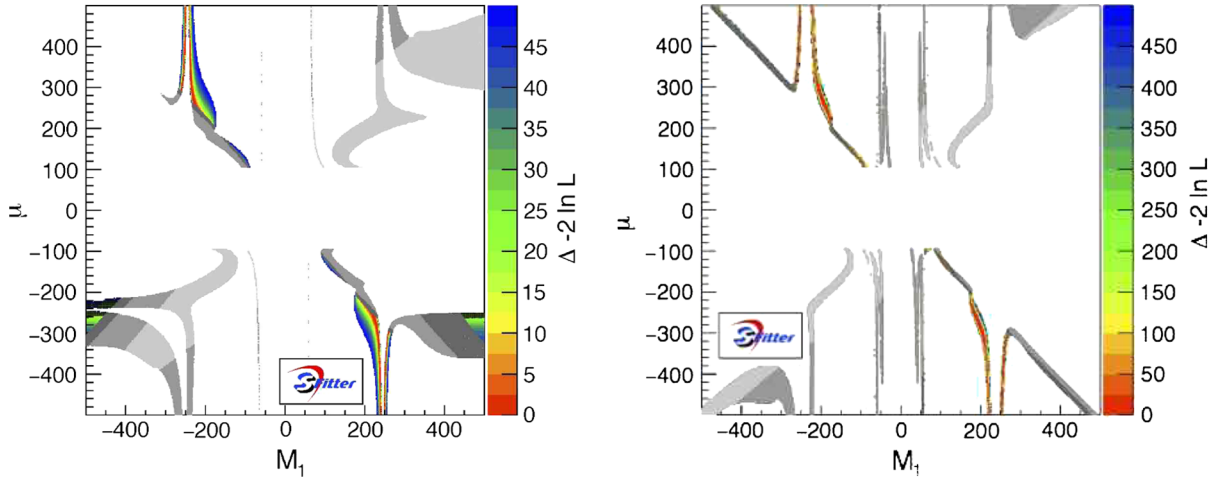

FIG. 9. Log-likelihood map including the GC excess, combined with Fermi-LAT limits from dwarf spheroidal galaxies and direct detection constraints (left) and after adding the relic density, and other constraints discussed in the text (right). We fix $M_2 = 700$ GeV, $m_A = 500$ GeV, $\tan\beta = 3$, and vary M_1 and μ. Different shades of gray indicate (from light to dark) the most recent exclusion limits from Xenon 100, PandaX and LUX.

A key parameter is the mass of a dark matter candidate which simultaneously explains the observed relic density and the GC excess, and at the same time respects all constraints in Table I as well as those from direct detection experiments. In Fig. 10 we show all points with $\Delta(-2\log L) \lesssim 450$, colored according to the LSP mass $m_{\tilde{\chi}_1^0}$. In the left panel we fix $M_2 = 700$ GeV and $\tan\beta = 3$, as before. The low value of $m_A = 500$ GeV opens a $t\bar{t}$ annihilation region with $m_{\tilde{\chi}_1^0} \approx 200$ GeV. In addition we see a few allowed points with $m_{\tilde{\chi}_1^0} \lesssim 100$ GeV in the WW regime.

In the right panel of Fig. 10 we fix $M_2 = 120$ GeV, allowing for a significant wino fraction in the LSP. According to Eq. (1) the wino content generally allows for a sizable annihilation rate through a t-channel chargino, implying that the LSP mass after requiring the annihilation rate matching the GC excess as well as the observed relic density will never exceed 120 GeV. On the other hand, a Higgsino admixture can lead to lighter valid dark matter candidates. We again identify the very narrow h peak and the broader Z peak. They define the allowed parameter points with $m_{\tilde{\chi}_1^0} \approx 45$ GeV and $m_{\tilde{\chi}_1^0} \approx 63$ GeV. In addition, we see a non-resonant band of allowed points with $m_{\tilde{\chi}_1^0} = 100\ldots120$ GeV, with an annihilation into WW pairs. Annihilation into a pair of top quarks is kinematically impossible. Direct detection experiments have a weaker impact because gaugino mixtures have smaller couplings to the light Higgs.

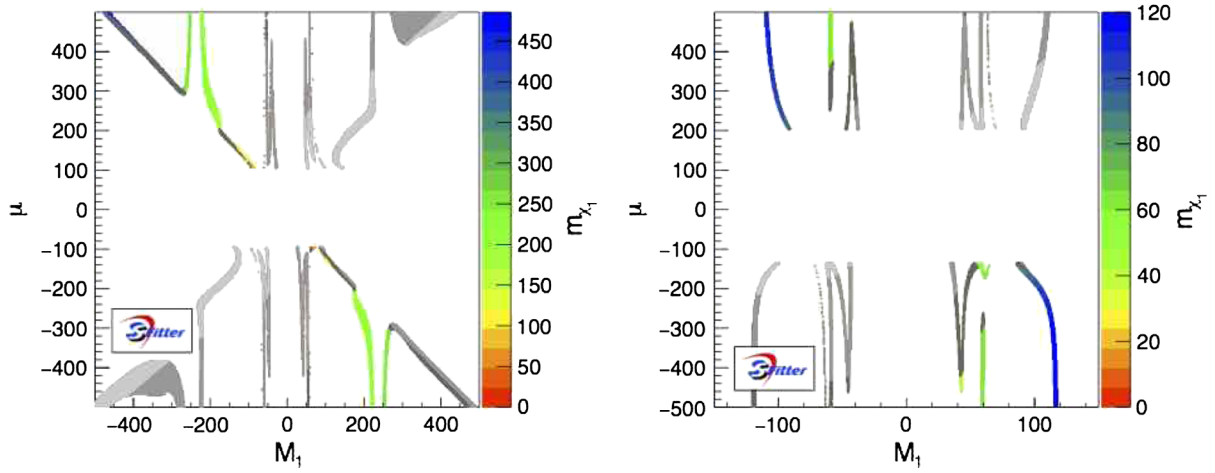

FIG. 10. Log-likelihood map including the Fermi-LAT photon spectrum, direct detection constraints, the observed relic density, and other constraints discussed in the text for fixed $m_A = 500$ GeV and $M_2 = 700$ GeV, $\tan\beta = 3$ (left) or $M_2 = 120$ GeV, $\tan\beta = 7$ (right). Different shades of gray indicate (from light to dark) the most recent exclusion limits from Xenon100, PandaX and LUX.

In summary, we see that in particular for a mixed wino-Higgsino LSP all three annihilation channels $b\bar{b}$, WW, $t\bar{t}$ survive current direct detection limits, but with a much reduced number of allowed parameter points. With the next generation of direct detection experiments it should be possible to probe these remaining MSSM parameter points.

B. Global parameter study

Finally, we perform a global MSSM fit in the neutralino/chargino parameter space. To assure the possibility of the heavy Higgs funnel we fix $m_A = 500$ GeV and vary:

$$|M_1| < 500\,\text{GeV} \quad |M_2| < 700\,\text{GeV} \quad |\mu| < 500\,\text{GeV}$$
$$|A_t| < 7\,\text{TeV} \quad \tan\beta = 2...45. \tag{5}$$

The remaining parameters, including squark masses, slepton masses, and trilinear couplings, are decoupled at 4 TeV. This choice allows for points interpolating between the two scenarios shown in Fig. 10: bino-Higgsino dark matter and wino-Higgsino dark matter. In addition, the simultaneous variation of $\tan\beta$ and A_t ensures that for any value of $\tan\beta$ we can generate the correct light Higgs mass while at the same time scanning the bottom Yukawa coupling or the width of the heavy Higgses.

In the upper panels of Fig. 11 we show the result of a global analysis taking into account all constraints defined in Table I, but not including direct detection bounds. For example the $\mu - M_1$ plane is now shown as a profile likelihood after projecting out the remaining model parameters. In general, this leads to a broadening of all features discussed before. We still see the usual narrow regions corresponding to the annihilation channels $\tilde{\chi}_1^0\tilde{\chi}_1^0 \to WW$ and $t\bar{t}$. In addition, broader structures for large $|\mu| \sim |M_1|$ are generated by the $\tan\beta$-enhanced annihilation $\tilde{\chi}_1^0\tilde{\chi}_1^0 \to A \to b\bar{b}$. They are much wider than all other structures because the heavy Higgs width scales with $\tan^2\beta$. In the second upper panel we observe that $\tan\beta$ has hardly any global effect on the annihilation rate, both for the GC excess and for the observed relic density. Towards large $\tan\beta$ we see how the low-M_1 scenarios reach a better agreement with data, and how the width of the pseudoscalar Higgs with $m_A = 500$ GeV increases. Finally, in the right panel we observe a strong correlation between M_2 and M_1, similar to the first panel, but with more washed-out structures in the profile likelihood. The Z funnel and h funnel are not resolved by the usual global analysis, and do not appear. From the previous discussion, it is clear that they are viable in the absence of direct detection constraints.

In the lower panels of Fig. 11 we add the LUX direct detection constraints. All general structures in the $\mu - M_1$ plane, corresponding to the different decay channels, survive. An independent sign change in μ and M_1 is no longer possible because of the large degree of fine-tuning. The main difference between this global result and the previous, two-dimensional analysis is that for large $\mu \sim -M_1$ the pseudoscalar Higgs funnel mediates an annihilation to $b\bar{b}$ pairs at large $\tan\beta$.

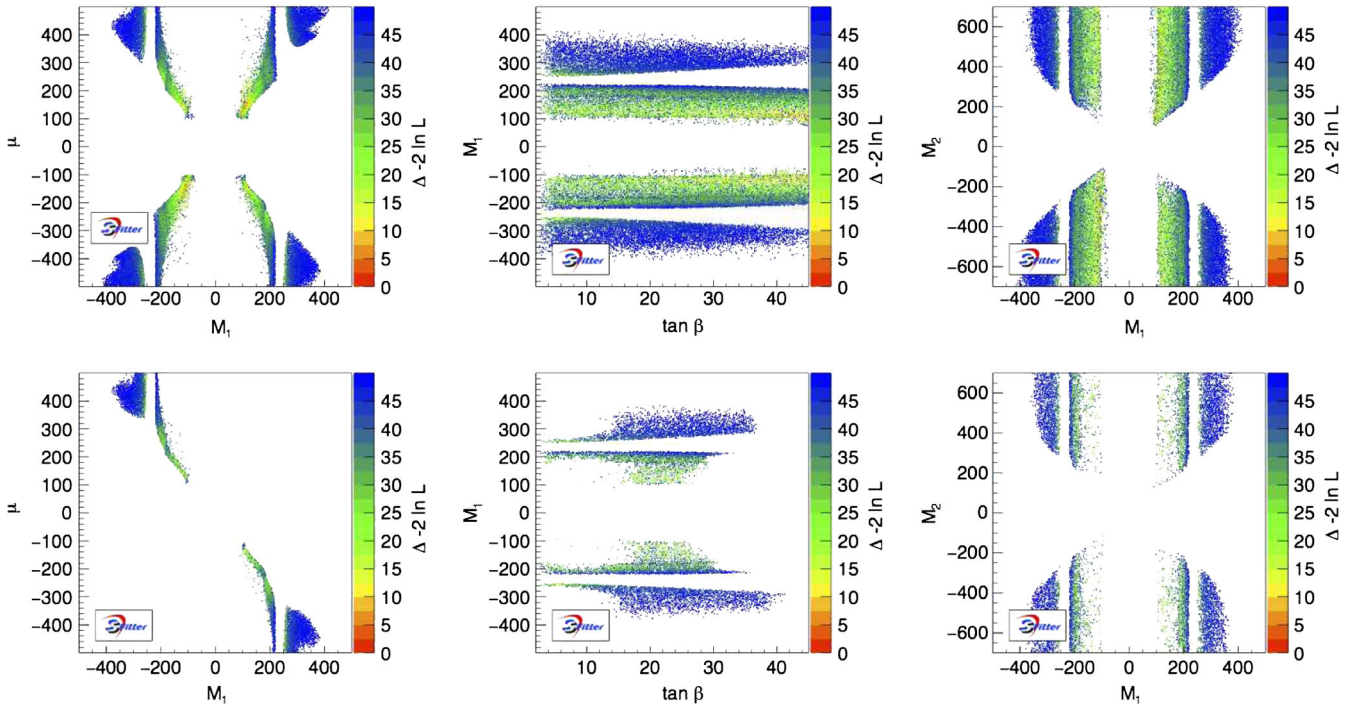

FIG. 11. Log-likelihood map for the combined Sfitter analysis of the Fermi-LAT photon spectrum, the observed relic density, and other constraints with (lower) and without (upper) including the LUX direct detection bounds.

Another new feature in the global fit is an allowed Higgsino LSP region for $M_1 = 100\ldots150$ GeV and $\tan\beta = 15\ldots25$. It corresponds to a combined annihilation to WW and ZZ pairs. Following Eq. (1) and Eq. (2) both, the $\tilde{\chi}_1^0 - \tilde{\chi}_1^\pm - W$ and $\tilde{\chi}_1^0 - \tilde{\chi}_1^0 - Z$ couplings increase for large $\tan\beta$. This way they lead to an efficient annihilation, but are also ruled out by direct detection constraints. When we reduce $\tan\beta \to 1$, the $\tilde{\chi}_1^0 - \tilde{\chi}_1^\pm - W$ coupling approaches a finite value, while the $\tilde{\chi}_1^0 - \tilde{\chi}_1^0 - Z$ vanishes.

V. OUTLOOK

Based on a realistic estimate of the different sources of uncertainty we have shown that the lightest neutralino in the MSSM can explain the Fermi-LAT GC excess. The different annihilation channels $\tilde{\chi}_1^0\tilde{\chi}_1^0 \to b\bar{b}$, WW, and $t\bar{t}$ define the corresponding LSPs with increasing masses. The annihilation channel $\tilde{\chi}_1^0\tilde{\chi}_1^0 \to hh$ does not work in the MSSM, because of the velocity suppression of the CP-even heavy Higgs funnel. Nevertheless, viable explanations of the GC excess in the MSSM can annihilate to a wide range of Standard Model states and cover a mass range from 45 GeV to well above 250 GeV.

If one demands that the LSP is a standard thermal relic, the preferred regions of parameter space slightly shift. The typical width of the structures in parameter space decreases significantly, corresponding to the small uncertainties from the *Planck* fits. Consequently, the allowed region of a combined SFitter analysis follows the patterns of the correct relic density. The best-fit region is again defined by the $b\bar{b}$, WW, and $t\bar{t}$ annihilation channels; it extends to LSP masses up to 300 GeV, in particular in combination with a pseudoscalar heavy Higgs mass around 500 GeV. In addition, we confirm two more features in the MSSM parameter space. First, a $\tan\beta$-enhanced annihilation of heavy neutralinos to $b\bar{b}$ pairs can be mediated by the pseudoscalar Higgs in complete analogy to the top quark case. Second, the different scaling of the neutral current and charged current couplings of the neutralino/chargino sector opens an allowed wino region for intermediate $\tan\beta$.

Finally, when we apply the full set of limits, the direct detection constraint cuts deeply into the allowed parameter space. Nevertheless, for a mixed wino-Higgsino LSP all three annihilation channels with their corresponding regions of parameter space survive. Most notably, a heavy neutralino annihilating to top or bottom pairs remains largely intact. Ignoring the relic density constraint and only considering the GC excess combined with direct detection constraints does not improve the situation qualitatively. All of our preferred regions of parameter space should be covered by the next generation of direct detection experiments.

ACKNOWLEDGMENTS

A. B. would like to thank the Heidelberg Graduate School for Fundamental Physics for her Ph.D. funding and the DFG Graduiertenkolleg *Particle Physics beyond the Standard Model* (Grant No. GK1940). T. P. and A. B. acknowledge the support by the DFG Forschergruppe *New Physics at the LHC* (Grant No. FOR2238). The work of S. M. is supported in part by U.S. Department of Energy Grant No. DE-SC0014431. The work of T. M. P. T. is supported in part by U.S. National Science Foundation Grant No. PHY-1620638.

[1] L. Goodenough and D. Hooper, Possible evidence For dark matter annihilation in the inner Milky Way from the Fermi Gamma Ray Space Telescope, arXiv:0910.2998; D. Hooper and L. Goodenough, Dark matter annihilation in the Galactic Center as seen by the Fermi Gamma Ray Space Telescope, Phys. Lett. B **697**, 412 (2011).

[2] D. Hooper and T. Linden, Origin of the gamma rays from the Galactic Center, Phys. Rev. D **84**, 123005 (2011); K. N. Abazajian and M. Kaplinghat, Detection of a Gamma-ray source in the Galactic Center consistent with extended emission from Dark Matter annihilation and concentrated astrophysical emission, Phys. Rev. D **86**, 083511 (2012); Erratum: Detection of a Gamma-ray source in the Galactic Center consistent with extended emission from Dark Matter annihilation and concentrated astrophysical emission, Phys. Rev. D **87**, 129902(E) (2013); D. Hooper and T. R. Slatyer, Two emission mechanisms in the Fermi bubbles: A possible signal of annihilating dark matter, Phys. Dark Universe **2**, 118 (2013); C. Gordon and O. Macias, Dark matter and pulsar model constraints from Galactic Center Fermi-LAT gamma ray observations, Phys. Rev. D **88**, 083521 (2013); Erratum: Dark matter and pulsar model constraints from Galactic Center Fermi-LAT gamma ray observations, Phys. Rev. D **89**, 049901(E) (2014); W. C. Huang, A. Urbano, and W. Xue, Fermi bubbles under dark matter scrutiny. Part I: Astrophysical analysis, arXiv:1307.6862; T. Daylan, D. P. Finkbeiner, D. Hooper, T. Linden, S. K. N. Portillo, N. L. Rodd, and T. R. Slatyer, The characterization of the gamma-ray signal from the central Milky Way: A case for annihilating dark matter, Phys. Dark Universe **12**, 1 (2016); K. N. Abazajian, N. Canac, S. Horiuchi, and M. Kaplinghat, Astrophysical and dark matter interpretations of extended Gamma-ray emission from the Galactic Center, Phys. Rev. D **90**, 023526 (2014); A. Alves, S. Profumo, F. S. Queiroz, and W. Shepherd, Effective field theory approach to the Galactic Center gamma-ray excess, Phys. Rev. D **90**,

115003 (2014); B. Zhou, Y.-F. Liang, X. Huang, X. Li, Y.-Z. Fan, L. Feng, and J. Chang, GeV excess in the Milky Way: The role of diffuse galactic gamma-ray emission templates, Phys. Rev. D **91**, 123010 (2015); F. Calore, I. Cholis, and C. Weniger, Background model systematics for the Fermi GeV excess, J. Cosmol. Astropart. Phys. 03 (2015) 038; K. N. Abazajian, N. Canac, S. Horiuchi, M. Kaplinghat, and A. Kwa, Discovery of a new Galactic Center excess consistent with upscattered starlight, J. Cosmol. Astropart. Phys. 07 (2015) 013; E. Carlson, T. Linden, and S. Profumo, Improved cosmic-ray injection models and the Galactic Center gamma-ray excess, Phys. Rev. D **94**, 063504 (2016).

[3] F. Calore, I. Cholis, C. McCabe, and C. Weniger, A tale of tails: Dark matter interpretations of the Fermi GeV excess in light of background model systematics, Phys. Rev. D **91**, 063003 (2015).

[4] M. Ajello *et al.* (Fermi-LAT Collaboration), Fermi-LAT observations of high-energy γ-ray emission toward the galactic center, Astrophys. J. **819**, 44 (2016).

[5] D. Hooper, I. Cholis, T. Linden, J. Siegal-Gaskins, and T. Slatyer, Pulsars cannot account for the inner Galaxy's GeV excess, Phys. Rev. D **88**, 083009 (2013); E. Carlson and S. Profumo, Cosmic ray protons in the inner galaxy and the Galactic Center gamma-ray excess, Phys. Rev. D **90**, 023015 (2014); J. Petrovic, P. D. Serpico, and G. Zaharijas, Galactic Center gamma-ray "excess" from an active past of the Galactic Centre?, J. Cosmol. Astropart. Phys. 10 (2014) 052; I. Cholis, D. Hooper, and T. Linden, Challenges in explaining the Galactic Center gamma-ray excess with millisecond pulsars, J. Cosmol. Astropart. Phys. 06 (2015) 043; I. Cholis, C. Evoli, F. Calore, T. Linden, C. Weniger, and D. Hooper, The Galactic Center GeV excess from a series of leptonic cosmic-ray outbursts, J. Cosmol. Astropart. Phys. 12 (2015) 005; E. Carlson, T. Linden, and S. Profumo, Improved cosmic-ray injection models and the Galactic Center gamma-ray excess, Phys. Rev. D **94**, 063504 (2016); O. Macias, C. Gordon, R. M. Crocker, B. Coleman, D. Paterson, S. Horiuchi, and M. Pohl, Discovery of gamma-ray emission from the X-shaped bulge of the Milky Way, arXiv:1611.06644.

[6] S. K. Lee, M. Lisanti, and B. R. Safdi, Distinguishing dark matter from unresolved point sources in the inner galaxy with photon statistics, J. Cosmol. Astropart. Phys. 05 (2015) 056; R. Bartels, S. Krishnamurthy, and C. Weniger, Strong Support for the Millisecond Pulsar Origin of the Galactic Center GeV Excess, Phys. Rev. Lett. **116**, 051102 (2016); S. K. Lee, M. Lisanti, B. R. Safdi, T. R. Slatyer, and W. Xue, Evidence for Unresolved γ-Ray Point Sources in the Inner Galaxy, Phys. Rev. Lett. **116**, 051103 (2016); S. D. McDermott, P. J. Fox, I. Cholis, and S. K. Lee, Wavelet-based techniques for the gamma-ray sky, J. Cosmol. Astropart. Phys. 07 (2016) 045.

[7] S. Horiuchi, M. Kaplinghat, and A. Kwa, Investigating the uniformity of the excess Gamma rays towards the Galactic Center region, J. Cosmol. Astropart. Phys. 11 (2016) 053.

[8] H. Goldberg, Constraint on the Photino Mass from Cosmology, Phys. Rev. Lett. **50**, 1419 (1983); M. Drees and M. M. Nojiri, The neutralino relic density in minimal $N = 1$ supergravity, Phys. Rev. D **47**, 376 (1993); J. R. Ellis, J. S. Hagelin, D. V. Nanopoulos, K. A. Olive, and M. Srednicki, Supersymmetric relics from the big bang, Nucl. Phys. **B238**, 453 (1984); G. Jungman, M. Kamionkowski, and K. Griest, Supersymmetric dark matter, Phys. Rep. **267**, 195 (1996); G. Bertone, D. Hooper, and J. Silk, Particle dark matter: Evidence, candidates, and constraints, Phys. Rep. **405**, 279 (2005); for an exceptionally beautiful set of plots on relic neutralinos see J. Bramante, P. J. Fox, A. Martin, B. Ostdiek, T. Plehn, T. Schell, and M. Takeuchi, Relic neutralino surface at a 100 TeV collider, Phys. Rev. D **91**, 054015 (2015).

[9] M. Cahill-Rowley, J. Gainer, J. Hewett, and T. Rizzo, Towards a supersymmetric description of the Fermi galactic center excess, J. High Energy Phys. 02 (2015) 057; T. Gherghetta, B. von Harling, A. D. Medina, M. A. Schmidt, and T. Trott, SUSY implications from WIMP annihilation into scalars at the Galactic Center, Phys. Rev. D **91**, 105004 (2015); R. Enberg, S. Munir, C. P. d. l. Heros, and D. Werder, Prospects for higgsino-singlino dark matter detection at IceCube and PINGU, arXiv:1506.05714; J. Cao, L. Shang, P. Wu, J. M. Yang, and Y. Zhang, Interpreting the Galactic Center gamma-ray excess in the NMSSM, arXiv:1506.06471; K. Freese, A. Lopez, N. R. Shah, and B. Shakya, MSSM A-funnel and the Galactic Center excess: Prospects for the LHC and direct detection experiments, J. High Energy Phys. 04 (2016) 059; M. van Beekveld, W. Beenakker, S. Caron, R. Peeters, and R. Ruiz de Austri, This year's holiday present: Supersymmetry with dark matter is still natural, arXiv:1612.06333.

[10] K. Hagiwara, S. Mukhopadhyay, and J. Nakamura, 10 GeV neutralino dark matter and light stau in the MSSM, Phys. Rev. D **89**, 015023 (2014).

[11] A. Berlin, D. Hooper, and S. D. McDermott, Simplified dark matter models for the Galactic Center gamma-ray excess, Phys. Rev. D **89**, 115022 (2014); M. Abdullah, A. DiFranzo, A. Rajaraman, T. M. P. Tait, P. Tanedo, and A. M. Wijangco, Hidden on-shell mediators for the Galactic Center γ-ray excess, Phys. Rev. D **90**, 035004 (2014); C. Balazs, T. Li, C. Savage, and M. White, Interpreting the Fermi-LAT gamma ray excess in the simplified framework, arXiv:1505.06758; M. Escudero, D. Hooper, and S. J. Witte, Updated collider and direct detection constraints on dark matter models for the Galactic Center gamma-ray excess, arXiv:1612.06462.

[12] D. K. Ghosh, S. Mondal, and I. Saha, Confronting the Galactic Center gamma ray excess with a light scalar dark matter, J. Cosmol. Astropart. Phys. 02 (2015) 035; A. Berlin, S. Gori, T. Lin, and L. T. Wang, Pseudoscalar portal dark matter, arXiv:1502.06000.

[13] C. Cheung, M. Papucci, D. Sanford, N. R. Shah, and K. M. Zurek, NMSSM interpretation of the Galactic Center excess, Phys. Rev. D **90**, 075011 (2014); J. Huang, T. Liu, L. T. Wang, and F. Yu, Supersymmetric subelectroweak scale dark matter, the Galactic Center gamma-ray excess, and exotic decays of the 125 GeV Higgs boson, Phys. Rev. D **90**, 115006 (2014); J. Guo, J. Li, T. Li, and A. G. Williams, NMSSM explanations of the Galactic Center gamma ray excess and promising LHC searches, Phys. Rev. D **91**, 095003 (2015); J. Cao, L. Shang, P. Wu, J. M. Yang, and Y. Zhang, Supersymmetry explanation of the Fermi Galactic Center excess and its test at LHC run II, Phys. Rev. D **91**, 055005 (2015); X. J. Bi, L. Bian,

W. Huang, J. Shu, and P. F. Yin, The interpretation for Galactic Center excess and electroweak phase transition in the NMSSM, arXiv:1503.03749.

[14] A. Butter, T. Plehn, M. Rauch, D. Zerwas, S. Henrot-Versille, and R. Lafaye, Invisible Higgs decays to hooperons in the NMSSM, Phys. Rev. D **93**, 015011 (2016).

[15] For an analysis based on preliminary Fermi-LAT results see e.g., P. Agrawal, B. Batell, P. J. Fox, and R. Harnik, WIMPs at the Galactic Center, J. Cosmol. Astropart. Phys. 05 (2015) 011.

[16] R. Lafaye, T. Plehn, M. Rauch, and D. Zerwas, Measuring supersymmetry, Eur. Phys. J. C **54**, 617 (2008); C. Adam, J.-L. Kneur, R. Lafaye, T. Plehn, M. Rauch, and D. Zerwas, Measuring unification, Eur. Phys. J. C **71**, 1 (2011); E. Turlay, R. Lafaye, T. Plehn, M. Rauch, and D. Zerwas, Measuring supersymmetry with heavy scalars, J. Phys. G **38**, 035003 (2011).

[17] S. Henrot-Versille, R. Lafaye, T. Plehn, M. Rauch, D. Zerwas, S. Plaszczynski, B. Rouille d'Orfeuil, and M. Spinelli, Constraining supersymmetry using the relic density and the Higgs boson, Phys. Rev. D **89**, 055017 (2014).

[18] S. Liem, G. Bertone, F. Calore, R. Ruiz de Austri, T. M. P. Tait, R. Trotta, and C. Weniger, Effective field theory of dark matter: A global analysis, J. High Energy Phys. 09 (2016) 077; C. Karwin, S. Murgia, T. M. P. Tait, T. A. Porter, and P. Tanedo, Dark matter interpretation of the Fermi-LAT observation toward the Galactic Center, arXiv:1612.05687.

[19] A. Achterberg, S. Amoroso, S. Caron, L. Hendriks, R. Ruiz de Austri, and C. Weniger, A description of the Galactic Center excess in the minimal supersymmetric standard model, J. Cosmol. Astropart. Phys. 08 (2015) 006; A. Achterberg, S. Caron, L. Hendriks, R. Ruiz de Austri, and C. Weniger, A description of the Galactic Center excess in the minimal supersymmetric standard model, arXiv:1502.05703; G. Bertone, F. Calore, S. Caron, R. Ruiz, J. S. Kim, R. Trotta, and C. Weniger, Global analysis of the pMSSM in light of the Fermi GeV excess: Prospects for the LHC Run-II and astroparticle experiments, J. Cosmol. Astropart. Phys. 04 (2016) 037.

[20] For the similar FITTINO approach see e.g., P. Bechtle, K. Desch, and P. Wienemann, Fittino: A program for determining MSSM parameters from collider observables using an iterative method, Comput. Phys. Commun. **174**, 47 (2006); P. Bechtle, T. Bringmann, K. Desch, H. Dreiner, M. Hamer, C. Hensel, M. Krämer, N. Nguyen *et al.*, Constrained Supersymmetry after two years of LHC data: A global view with Fittino, J. High Energy Phys. 06 (2012) 098.

[21] A. Höcker, H. Lacker, S. Laplace, and F. Le Diberder, A new approach to a global fit of the CKM matrix, Eur. Phys. J. C **21**, 225 (2001).

[22] M. Ackermann *et al.* (Fermi-LAT Collaboration), The Fermi large area telescope on orbit: Event classification, instrument response functions, and calibration, Astrophys. J. Suppl. Ser. **203**, 4 (2012).

[23] K. N. Abazajian and R. E. Keeley, Bright gamma-ray Galactic Center excess and dark dwarfs: Strong tension for dark matter annihilation despite Milky Way halo profile and diffuse emission uncertainties, Phys. Rev. D **93**, 083514 (2016).

[24] A. Djouadi, J.-L. Kneur, and G. Moultaka, SuSpect: A Fortran code for the supersymmetric and Higgs particle spectrum in the MSSM, Comput. Phys. Commun. **176**, 426 (2007); G. Brooijmans *et al.*, Les Houches 2011: Physics at TeV colliders New Physics Working Group report, arXiv:1203.1488.

[25] A. Djouadi, J. Kalinowski, and M. Spira, HDECAY: A Program for Higgs boson decays in the standard model and its supersymmetric extension, Comput. Phys. Commun. **108**, 56 (1998); M. Mühlleitner, A. Djouadi, and Y. Mambrini, SDECAY: A Fortran code for the decays of the supersymmetric particles in the MSSM, Comput. Phys. Commun. **168**, 46 (2005); A. Djouadi, M. M. Mühlleitner, and M. Spira, Decays of supersymmetric particles: The program SUSY-HIT (SUspect-SdecaY-Hdecay-InTerface), Acta Phys. Pol. B **38**, 635 (2007).

[26] G. Belanger, F. Boudjema, P. Brun, A. Pukhov, S. Rosier-Lees, P. Salati, and A. Semenov, Indirect search for dark matter with micrOMEGAs2.4, Comput. Phys. Commun. **182**, 842 (2011).

[27] T. Cohen and J. G. Wacker, Here be dragons: The unexplored continents of the CMSSM, J. High Energy Phys. 09 (2013) 061.

[28] See e.g., A. Fowlie, K. Kowalska, L. Roszkowski, E. M. Sessolo, and Y.-L. S. Tsai, Dark matter and collider signatures of the MSSM, Phys. Rev. D **88**, 055012 (2013); C. Strege, G. Bertone, F. Feroz, M. Fornasa, R. Ruiz de Austri, and R. Trotta, Global Fits of the cMSSM and NUHM including the LHC Higgs discovery and new XENON100 constraints, J. Cosmol. Astropart. Phys. 04 (2013) 013; B. Bhattacherjee, M. Chakraborti, A. Chakraborty, U. Chattopadhyay, D. Das, and D. K. Ghosh, Implications of 98 GeV and 125 GeV Higgs scenario in nondecoupling SUSY with updated ATLAS, CMS and PLANCK data, arXiv:1305.4020; M. Cahill-Rowley, J. Hewett, A. Ismail, and T. Rizzo, Constraints on Higgs properties and SUSY partners in the pMSSM, arXiv:1308.0297; O. Buchmüller, R. Cavanaugh, M. Citron, A. De Roeck, M. J. Dolan, J. R. Ellis, H. Flacher, S. Heinemeyer *et al.*, The CMSSM and NUHM1 in Light of 7 TeV LHC, $B_s \to \mu^+\mu^-$ and XENON100 data, Eur. Phys. J. C **72**, 2243 (2012); etc.

[29] M. Bauer, A. Butter, N. Desai, J. Gonzalez-Fraile, and T. Plehn, On the validity of dark matter effective theory, arXiv:1611.09908.

[30] K. Griest and D. Seckel, Three exceptions in the calculation of relic abundances, Phys. Rev. D **43**, 3191 (1991); S. Mizuta and M. Yamaguchi, Coannihilation effects and relic abundance of Higgsino dominant LSP(s), Phys. Lett. B **298**, 120 (1993); J. R. Ellis, T. Falk, and K. A. Olive, Neutralino-stau coannihilation and the cosmological upper limit on the mass of the lightest supersymmetric particle, Phys. Lett. B **444**, 367 (1998).

[31] P. Binetruy, G. Girardi, and P. Salati, Constraints on a system of two neutral fermions from cosmology, Nucl. Phys. **B237**, 285 (1984); S. Mizuta and M. Yamaguchi, Coannihilation effects and relic abundance of Higgsino dominant LSP(s), Phys. Lett. B **298**, 120 (1993).

[32] C. Boehm, A. Djouadi, and M. Drees, Light scalar top quarks and supersymmetric dark matter, Phys. Rev. D **62**, 035012 (2000).

[33] ALEPH Collaboration, Search for scalar leptons in e^+e^- collisions at centre-of-mass energies up to 209 GeV, Phys. Lett. B **526**, 206 (2002); Absolute mass lower limit for the lightest neutralino of the MSSM from e^+e^- data at s up to 209 GeV, Phys. Lett. B **583**, 247 (2004); DELPHI Collaboration, Eur. Phys. J. C **31**, 421 (2003); L3 Collaboration, Search for scalar leptons and scalar quarks at LEP, Phys. Lett. B **580**, 37 (2004); OPAL Collaboration, Search for anomalous production of di-lepton events with missing transverse momentum in e^+e^- collisions at $\sqrt{s} = 183$–$209\times$ GeV, Eur. Phys. J. C **32**, 453 (2004); ALEPH Collaboration, Search for scalar quarks in e^+e^- collisions at s up to 209 GeV, Phys. Lett. B **537**, 5 (2002); OPAL Collaboration, Search for scalar top and scalar bottom quarks at LEP, Phys. Lett. B **545**, 272 (2002); ALEPH Collaboration, Search for charginos nearly mass degenerate with the lightest neutralino in e^+e^- collisions at centre-of-mass energies up to 209 GeV, Phys. Lett. B **533**, 223 (2002); L3 Collaboration, Searches for scalar quarks in e^+e^- interactions at s = 189 GeV, Phys. Lett. B **471**, 308 (1999); LEP2 SUSY Working Group, ALEPH, DELPHI, L3 and OPAL experiments.

[34] J. Bramante, N. Desai, P. Fox, A. Martin, B. Ostdiek, and T. Plehn, Towards the final word on neutralino dark matter, Phys. Rev. D **93**, 063525 (2016).

[35] For a recent update see A. Freitas, Higher-order electroweak corrections to the partial widths and branching ratio, J. High Energy Phys. 04 (2014) 070.

[36] For the updated LHC see e.g., C. Bernaciak, T. Plehn, P. Schichtel, and J. Tattersall, Spying an invisible Higgs boson, Phys. Rev. D **91**, 035024 (2015).

[37] M. Ackermann *et al.* (Fermi-LAT Collaboration), Searching for Dark Matter Annihilation from Milky Way Dwarf Spheroidal Galaxies with Six Years of Fermi Large Area Telescope Data, Phys. Rev. Lett. **115**, 231301 (2015).

[38] D. M. Pierce, J. A. Bagger, K. T. Matchev, and R. j. Zhang, Precision corrections in the minimal supersymmetric standard model, Nucl. Phys. **B491**, 3 (1997); T. Fritzsche and W. Hollik, Complete one loop corrections to the mass spectrum of charginos and neutralinos in the MSSM, Eur. Phys. J. C **24**, 619 (2002); W. Oller, H. Eberl, W. Majerotto, and C. Weber, Analysis of the chargino and neutralino mass parameters at one loop level, Eur. Phys. J. C **29**, 563 (2003).

[39] U. Baur, T. Plehn, and D. L. Rainwater, Probing the Higgs self-coupling at hadron colliders using rare decays, Phys. Rev. D **69**, 053004 (2004).

[40] A. Cuoco, B. Eiteneuer, J. Heisig, and M. Krämer, A global fit of the γ-ray galactic center excess within the scalar singlet Higgs portal model, J. Cosmol. Astropart. Phys. 06 (2016) 050.

[41] E. Aprile *et al.* (XENON100 Collaboration), Dark Matter Results from 100 Live Days of XENON100 Data, Phys. Rev. Lett. **107**, 131302 (2011); E. Aprile *et al.* (XENON100 Collaboration), Dark Matter Results from 225 Live Days of XENON100 Data, Phys. Rev. Lett. **109**, 181301 (2012).

[42] D. S. Akerib *et al.* (LUX Collaboration), Results from a search for dark matter in the complete LUX exposure, arXiv:1608.07648.

[43] A. Tan *et al.* (PandaX-II Collaboration), Dark Matter Results from First 98.7 Days of Data from the PandaX-II Experiment, Phys. Rev. Lett. **117**, 121303 (2016).

[44] ATLAS and CMS Collaborations, Combined Measurement of the Higgs Boson Mass in pp Collisions at $\sqrt{s} = 7$ and 8 TeV with the ATLAS and CMS Experiments, Phys. Rev. Lett. **114**, 191803 (2015).

[45] For a short history of MSSM studies see e.g., M. S. Carena, J. R. Espinosa, M. Quiros, and C. E. M. Wagner, Analytical expressions for radiatively corrected Higgs masses and couplings in the MSSM, Phys. Lett. B **355**, 209 (1995); H. E. Haber, R. Hempfling, and A. H. Hoang, Approximating the radiatively corrected Higgs mass in the minimal supersymmetric model, Z. Phys. C **75**, 539 (1997); S. Heinemeyer, W. Hollik, and G. Weiglein, The masses of the neutral *CP*-even Higgs bosons in the MSSM: Accurate analysis at the two loop level, Eur. Phys. J. C **9**, 343 (1999); G. Degrassi, S. Heinemeyer, W. Hollik, P. Slavich, and G. Weiglein, Towards high-precision predictions for the MSSM Higgs sector, Eur. Phys. J. C **28**, 133 (2003); P. Kant, R. V. Harlander, L. Mihaila, and M. Steinhauser, Light MSSM Higgs boson mass to three-loop accuracy, J. High Energy Phys. 08 (2010) 104; T. Hahn, S. Heinemeyer, W. Hollik, H. Rzehak, and G. Weiglein, High-Precision Predictions for the Light *CP*-Even Higgs Boson Mass of the Minimal Supersymmetric Standard Model, Phys. Rev. Lett. **112**, 141801 (2014); E. Bagnaschi, R. V. Harlander, S. Liebler, H. Mantler, P. Slavich, and A. Vicini, Towards precise predictions for Higgs-boson production in the MSSM, J. High Energy Phys. 06 (2014) 167; G. Degrassi, S. Di Vita, and P. Slavich, Two-loop QCD corrections to the MSSM Higgs masses beyond the effective-potential approximation, Eur. Phys. J. C **75**, 61 (2015).

[46] P. A. R. Ade *et al.* (Planck Collaboration), Planck 2015 results. XIII. Cosmological parameters, arXiv:1502.01589.

[47] G. W. Bennett *et al.*, Measurement of the positive Muon anomalous magnetic moment to 0.7 ppm, Phys. Rev. Lett. **89**, 101804 (2002); Erratum, Phys. Rev. Lett. **89**, 129903(E) (2002); Measurement of the negative Muon anomalous magnetic moment to 0.7 ppm, Phys. Rev. Lett. **92**, 161802 (2004); Final report of the E821 muon anomalous magnetic moment measurement at BNL, Phys. Rev. D **73**, 072003 (2006).

[48] CLEO Collaboration, Branching Fraction and Photon Energy Spectrum for $b \to s\gamma$, Phys. Rev. Lett. **87**, 251807 (2001); *BABAR* Collaboration, Measurement of $\mathcal{B}(B \to X_s\gamma)$, the $B \to X_s\gamma$ photon energy spectrum, and the direct CP asymmetry in $B \to X_{s+d}\gamma$ decays, Phys. Rev. D **86**, 112008 (2012); Belle Collaboration, Measurement of Inclusive Radiative B-Meson Decays with a Photon Energy Threshold of 1.7 GeV, Phys. Rev. Lett. **103**, 241801 (2009); J. Beringer *et al.* (Particle Data Group), Review of Particle Physics, Phys. Rev. D **86**, 010001 (2012).

[49] LHCb Collaboration, First Evidence for the Decay $B_s^0 \to \mu^+\mu^-$, Phys. Rev. Lett. **110**, 021801 (2013); CMS Collaboration, Measurement of the $B_s^0 \to \mu^+\mu^-$ Branching Fraction and Search for $B_s^0 \to \mu^+\mu^-$ with the CMS Experiment, Phys. Rev. Lett. **111**, 101804 (2013); CMS and LHCb Collaborations, Observation of the rare $B_s^0 \to \mu^+\mu^-$ decay from the combined analysis of CMS and LHCb data, Nature (London) **522**, 68 (2015).